Monthly Notices
of the
ROYAL ASTRONOMICAL SOCIETY

MNRAS **460,** 2193–2206 (2016)
Advance Access publication 2016 May 11

doi:10.1093/mnras/stw1114

Dynamical analysis of the cluster pair: A3407 + A3408

R. S. Nascimento,[1,2⋆] A. L. B. Ribeiro,[2⋆] M. Trevisan,[3,4] E. R. Carrasco,[5] H. Plana[2] and R. Dupke[6,7,8]

[1]*Observatório do Valongo, Universidade Federal do Rio de Janeiro, Rio de Janeiro-RJ, Brasil*
[2]*Laboratório de Astrofísica Teórica e Observacional, Universidade Estadual de Santa Cruz – 45650-000, Ilhéus-BA, Brasil*
[3]*Instituto Nacional de Pesquisas Espaciais, São José dos Campos-SP, Brasil*
[4]*Institut d'Astrophysique de Paris (UMR 7095: CNRS and UPMC), 98 bis Bd Arago, F-75014 Paris, France*
[5]*Gemini Observatory, Southern Operations Center, AURA, Casilla 603, La Serena, Chile*
[6]*Observatório Nacional, CP 20921-400, Rio de Janeiro-RJ, Brasil*
[7]*Department of Astronomy, University of Michigan, 500 Church St, Ann Arbor, MI 48109, USA*
[8]*Eureka Scientific Inc., 2452 Delmer St Suite 100, Oakland, CA 94602, USA*

Accepted 2016 May 9. Received 2016 May 9; in original form 2016 April 11

ABSTRACT

We carried out a dynamical study of the galaxy cluster pair A3407 and A3408 based on a spectroscopic survey obtained with the 4 metre Blanco telescope at the Cerro Tololo Inter-american Observatory, plus 6dF data, and *ROSAT* All-Sky Survey. The sample consists of 122 member galaxies brighter than $m_R = 20$. Our main goal is to probe the galaxy dynamics in this field and verify if the sample constitutes a single galaxy system or corresponds to an ongoing merging process. Statistical tests were applied to clusters members showing that both the composite system A3407 + A3408 as well as each individual cluster have Gaussian velocity distribution. A velocity gradient of $\sim$847 $\pm$ 114 km s^{-1} was identified around the principal axis of the projected distribution of galaxies, indicating that the global field may be rotating. Applying the KMM algorithm to the distribution of galaxies, we found that the solution with two clusters is better than the single unit solution at the 99 per cent cl. This is consistent with the X-ray distribution around this field, which shows no common X-ray halo involving A3407 and A3408. We also estimated virial masses and applied a two-body model to probe the dynamics of the pair. The more likely scenario is that in which the pair is gravitationally bound and probably experiences a collapse phase, with the cluster cores crossing in less than $\sim 1\,h^{-1}$ Gyr, a pre-merger scenario. The complex X-ray morphology, the gas temperature, and some signs of galaxy evolution in A3408 suggest a post-merger scenario, with cores having crossed each other $\sim 1.65\,h^{-1}$ Gyr ago, as an alternative solution.

Key words: galaxies: clusters: general – galaxies: clusters: intracluster medium – galaxies: evolution – galaxies: statistics.

1 INTRODUCTION

Clusters of galaxies are good tracers of the large-scale distribution of matter. They are the largest gravitationally bound systems in the Universe, constraining both structure formation and the composition of the Universe (e.g. Voit 2005; Allen, Evrard & Mantz 2011; Kravtsov & Borgani 2012). These systems also constitute important environments for the study of galaxy formation and evolution. In the hierarchical scenario, clusters are relatively recent structures collapsing at $z \lesssim 2$ (e.g. Cohn & White 2005), and growing at the intersections of cosmic filaments (e.g. Springel et al. 2005; Araya-Melo et al. 2009). In the Λcold dark matter (CDM) scenario, structures form in a bottom-up fashion: more massive galaxy systems assemble their mass from the merging of less massive ones (e.g. De Lucia, Springel & White 2006; Naab, Johansson & Ostriker 2007; Cattaneo, Mamon & Warnick 2011). Continuous galaxy interaction for period longer than the relaxation time tend to distribute the velocities of the galaxy members towards a Gaussian distribution (e.g. Bird & Beers 1993). This provides a way to access the dynamical state of galaxy clusters by studying their velocity distributions. Usually, distributions are well approximated by a Gaussian in the virialized (more central) regions of clusters (e.g. Yahil & Vidal 1977), while in peripheral areas, they can show

⋆ E-mail: rnascimento@astro.ufrj.br (RSN); albr@uesc.br (ALBR)

deviations from Gaussianity (e.g. Ribeiro, Lopes & Trevisan 2011). This indicates that the central parts are probably in dynamical equilibrium, when outskirts continue to accumulate matter from the surroundings. This accretion of matter, in the form of galaxies or groups of galaxies from the neighbourhood, seems to occur along giant filamentary structures (e.g. Krause, Ribeiro & Lopes 2013). This suggests that the formation of a galaxy cluster is a continuous process that takes place through mergers and encounters in greater or lesser proportions. Some outstanding examples of this are the so-called Bullet Cluster (1E 0657-56; Clowe, Bradac & Gonzalez 2006; Jee et al. 2007), and other clusters like Cl 0152-1357, MS 1054 (Jee et al. 2005a,b), and Abell 520 (Markevitch et al. 2005; Mahdavi et al. 2007).

To understand the impact of mergers on cluster evolution, it is important to study the process at different epochs. In the literature, only a few early merging clusters have been found up to now (Kato et al. 2015). Examples of this are the pairs Abell 222-223 (e.g. Werner et al. 2008), and Abell 399-401 (e.g. Fujita et al. 1996, 2008). Systems like Abell 3407-3408 (hereafter A3407-A3408), relatively isolated in the field, may provide an invaluable opportunity to study early signatures of merging clusters. This pair lies in a largely unexplored low galactic latitude section ($b \approx 17\overset{\circ}{.}57$) of the southern sky, where just few optical and X-ray observations have been performed. All available information may be summarized as follows: (i) the morphological classification of A3407 and A3408 is Bautz–Morgan type I, and type I-II, respectively (Abell, Corwin & Olowin 1989), suggesting that they are relaxed to moderately relaxed systems. (ii) On the other hand, the study of Galli et al. (1993) suggests that A3407 and A3408 are interacting and may form a single system. (iii) Campusano & Hardy (1996) discovered an arc-like feature ($z = 0.073$) near to the centre of A3408. This result was further confirmed by Campusano, Kneib & Hardy (1998) and Cypriano et al. (2001). (iv) The pair has been detected by the *ROSAT* All-Sky Survey (Ebeling et al. 1996) and A3408 by ASCA (Katayama, Hayashida & Hashimotodani 2001). (v) Finally, the estimated mass of A3408, evaluated from ASCA X-ray observations and enclosed within the arc radius, represents 18 per cent–45 per cent of the dynamical mass computed by Campusano et al. (1998). In their estimation, Campusano et al. (1998) assume that the centre of the cluster potential coincides with the brightest cluster galaxy (BCG), when this one is ∼60 arcsec off the X-ray centre (Katayama et al. 2001).

In this work, we present new radial velocities for galaxies around the galaxy cluster pair A3407 and A3408. Our main goal is to probe the galaxy dynamics in this field and verify if the sample constitutes a single galaxy system or corresponds to an ongoing merging process, improving the understanding of this system. The paper is organized as follows: in Section 2, we present the observations, data reduction and the methodology used to find the galaxy redshifts; in Section 3, we present a study of the velocity distribution, covering membership determination, normality tests, and identification of significant gaps; in Section 4, we study subclustering in the field; in Section 5, we present a dynamical analysis, covering the virialization properties and the two-body model applied to the pair A3407-A3408; and in Section 6, we discuss our results.[1]

2 OBSERVATIONS AND DATA REDUCTION

2.1 Observations

All images and spectroscopic data of Abell 3407 and Abell 3408 were collected with the 4 metre Victor Blanco telescope at the Cerro Tololo Interamerican Observatory (CTIO), in Chile. The clusters were imaged through the *B*, *V* and *R* Johnson–Cousins filters with the Mosaic II CCD imager during the nights of 2007 February 14 and 15. The Mosaic II array is composed by eight 2048 × 4096 SITe CCDs. With a pixel size of 15 μm and a scale of 0.27 arcsec pix^{-1}, the Mosaic II array cover an area of ∼38 arcmin^2 on the sky (equivalent to about 1.8 × 1.8 Mpc^2 at the distance of the Abell 3407/Abell 3408 clusters). For Abell 3407, a total of 7 × 300 s exposures in *R* filter and 3 × 300 exposures in *B* and *V* filters were obtained, given an effective exposure times of 2100 s for *R* filter and 900 s for *B* and *V* filters, respectively. For Abell 3408, a total of 4 × 300 s exposure in all three filters were obtained, given an effective exposure time of 1200 s for all filters. Abell 3407 was observed under photometric conditions while Abell 3408 was observed under non-photometric conditions (patchy cloudy). The two clusters were observed with a small overlap (∼1 arcmin) to allow us to calibrate the observations of Abell 3408. The seeing conditions were poor to average in both nights, with a seeing that varied between 0.9 arcsec to 1.6 arcsec (DIMM monitor). Offsets between exposures were used to take into account the gaps between the CCDs and for calibration errors. In Fig. 1, we show the pre-images fields of A3407+A3408 in the *R* band. The total field is around 73 arcmin.

The optical spectra of objects in Abell 3407 and 3408 were obtained with the Hydra-CTIO multiobject spectrograph (Barden & Ingerson 1998) on 2007 April 12, during dark time, with a good transparency, and with a seeing that varied between 0.5 and 0.8 arcsec (DIMM monitor). The spectra were acquired using the KPGL2 grating over the wavelength range 3450–8242 Å, centred in 5845 Å, which provided a spectral resolution of ∼6.5 Å, and a dispersion of 2.33 Å pixel^{-1}. To avoid second-order contamination above 8000 Å, the blocking filter GG385 was used. All spectra were imaged with the 400 mm Bench Schmidt camera on to a SITe 2k × 4k CCD, with a binning of 2 pixels in the spectral direction. Total exposure times of 3 × 1800 s and 3 × 1500 s were used for the objects observed in the region of Abell 3407 and Abell 3408, respectively.

2.2 Data reduction

The observations were processed with the MSCRED package inside IRAF.[2] The images were bias/overscan-subtracted, trimmed and flat-fielded. The processed images were then registered to a common pixel position and median combined. Calibration on the standard *B*, *V* and *R* magnitude system for Abell 3407 was achieved using observation of stars from Landolt (1992). Stars in the overlap region between the two clusters were used to calibrate the photometry in the field of Abell 3408. The accuracy of the calibrations was of the order of 5 per cent and 7 per cent for *B*, *V* and *R* filters, respectively.

The galaxies used for spectroscopic follow-up were selected using the (*B*−*R*) versus *R* colour–magnitude diagram. We performed selection of the targets using the SOURCE EXTRACTOR software version 2.5 (Bertin & Arnouts 1996), for both *B* and *R* images, taking into account only objects whose galaxy–star separation was 0.3.

[1] Throughout this paper, we assume a ΛCDM cosmology with the cosmological parameters $\Omega_M = 0.3$, $\Omega_\Lambda = 0.7$ and $H_0 = 100$ h km s^{-1} Mpc^{-1}.

[2] IRAF is distributed by NOAO, which is operated by the Association of Universities for Research in Astronomy Inc., under cooperative agreement with the National Science Foundation.

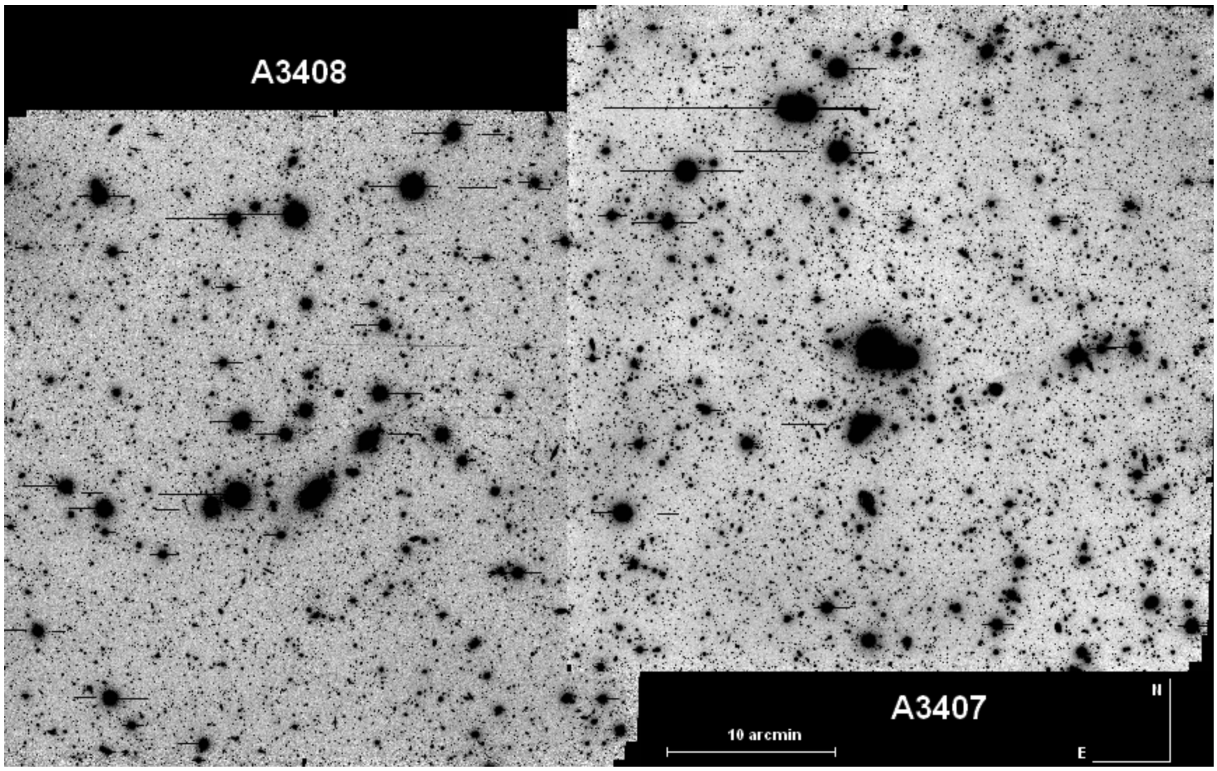

Figure 1. Pre-images fields of A3407+A3408 in the *R* band. The total field is around 73 arcmin.

Furthermore, we selected the targets which are in colour range $0 < B{-}R < 2.5$ and brighter than $R = 20$ from colour–magnitude diagram, $(B{-}R)$ versus R.

The spectroscopic observations were reduced using the standard procedures in IRAF. All science exposure, comparison lamps (He–Ne–Ar), spectroscopic flats and 'milk-flats' were bias/overscan-subtracted and trimmed using the CCDRED package. The 'milki-flats' were combined and spectral shapes in *x*- and *y*-direction were removed using the task FIT1D. The resultant image was then filtered by using a median filter and normalized to one. The science exposures and spectroscopic flats were then divided by the processed 'milk flats' in order to reduce spectral noise in the images.

Cosmic rays removals was performed in the 2D-processed images using the LAPLACIAN COSMIC RAY IDENTIFICATION program[3] (van Dokkum 2001). The spectra were extracted with DOHYDRA task inside the IRAF HYDRA package. Dome flats were used to flat-field the individual fibers, while twilight flats were used for fibre to fibre throughput correction. The spectra were then wavelength-calibrated. The residual values in the wavelength solution for 20–30 points using a fourth- or fifth-order Chebyshev polynomial typically yielded rms values of ∼0.20–0.50 Å. Finally, the average sky spectrum was subtracted from each object spectrum using typically 12 sky fibre spectra per field.

2.3 Radial velocities

The radial velocities were determined with the IRAF RVSAO package (Kurtz & Mink 1998). The task EMSAO was used to compute the redshifts for spectra dominated by emission lines. For each identified line, a Gaussian profile is fitting and the radial velocity is computed. Then, the final radial velocity is determined by combining them into a single value. The spectra with observed absorption lines were correlated with 12 high signal-to-noise (S/N) stellar and galaxy templates from Carrasco, Mendes de Oliveira & Infante (2006) using the task XCSAO. The final heliocentric radial velocities and the *R* parameter (Tonry & Davis 1979), which gives the quality of the spectra are listed in Tables A1 and A2.

The following sources of uncertainties were taken into account in the velocity errors: the wavelength calibration errors; the internal error, which accounts for noise in the spectra; and the external error, introduced during the cross-correlation procedure. The first was determined from the wavelength solution, and the second was estimated from the dispersion in velocities obtained with different templates. The last, the external error, corresponds to the error returned by the XCSAO task corrected by a factor b, which was obtained as follows. Since there are no systematic velocity shifts between different exposures, measurements from different observations of the same object can be used to obtain the calibration factor. The normalized velocity shift is defined as

$$\delta v_{\rm n} = \frac{v_1 - v_2}{\sqrt{b^2(\sigma_1^2 + \sigma_2^2)}}, \quad (1)$$

where v_1, v_2 are the velocities determined from two different exposures, and σ_1, σ_2 are the errors returned by the cross-correlation program. The calibration factor b was obtained assuming that the distribution of the quantity $\delta v_{\rm n}$ must be Gaussian with dispersion 1.0 and folded about zero. Using the Kolmogorov–Smirnov test, we compared the distribution of the normalized velocity shifts, $\delta v_{\rm n}$, and the folded Gaussian. A satisfactory match between these two distributions is achieved if the errors are multiplied by $b = 0.8$

[3] http://www.astro.yale.edu/dokkum/lacosmic/

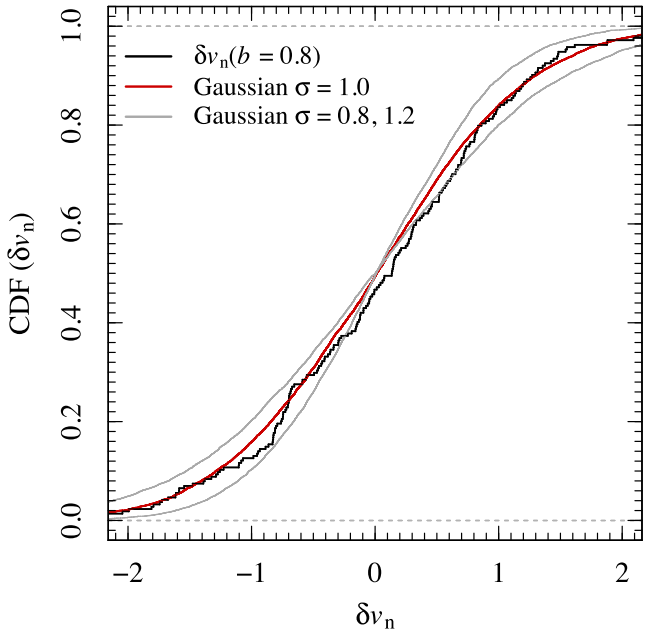

Figure 2. Cumulative distribution function (CDF) for the velocity shifts between measurements from different exposures, normalized by the XCSAO errors corrected by a factor b (δv_n, equation 1). For $b = 0.8$, there is a match between the CDF for this quantity and for the Gaussian distribution with $\sigma = 1.0$ (black and red lines, respectively). The grey lines indicate the CDF for the Gaussian distributions with $\sigma = 0.8$ and 1.2.

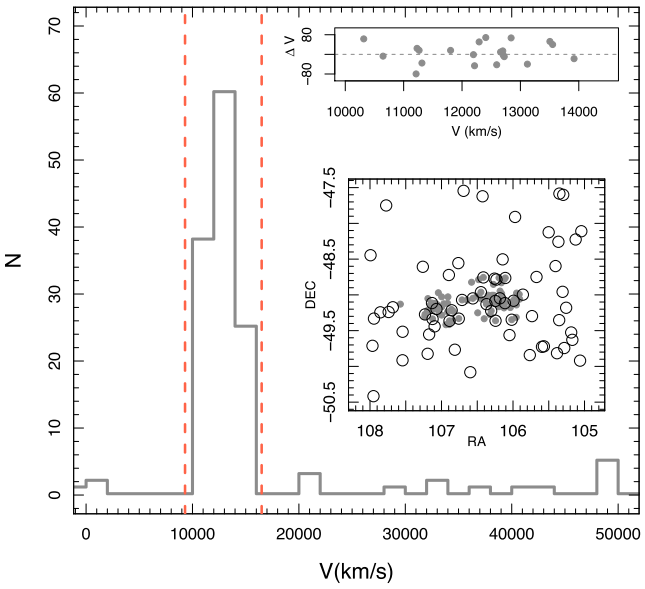

Figure 3. Velocity distribution before discarding outliers. Red dashed lines show the initial cut-off of $\pm 3000\,\mathrm{km\,s^{-1}}$ around the median redshift, $z_{cl} \approx 0.042$. The secondary panel shows the spatial distribution of our survey (grey filled circles) plus the 6dF data (open circles). The small upper panel shows the velocity comparison of the 21 objects common to our sample and 6dF.

(Fig. 2). This correction factor was applied to the XCSAO errors. The final error δv_{final} was obtained by adding in quadrature each error term. On average, we find $\langle \delta v_{final} \rangle \approx 53\,\mathrm{km\,s^{-1}}$.

3 VELOCITY DISTRIBUTION

Combining our spectroscopic observations with the data available at the 6dFGS[4] data base (Jones et al. 2009), we gathered radial velocities for 156 galaxies in the field of $\sim 3^\circ \times 3^\circ$ centred at the mid-distance between A3407 and A3408 (see Fig. 3). Of this total, there are 21 galaxies, identified as repeated objects, which were used to check consistency between the two redshift surveys. Computing the absolute difference between the two independent radial velocity measurements, we find $\langle |\Delta V| \rangle \approx 45\,\mathrm{km\,s^{-1}}$ on average (see Fig. 3). This quantity is a little smaller than $\langle \delta v_{final} \rangle$, indicating that our combined sample is internally consistent.

3.1 Membership, location and scale

All properties of galaxy clusters can be significantly affected by projection effects. Over the years, many methods have been developed to remove interlopers from galaxy clusters (e.g. Yahil & Vidal 1977; den Hartog & Katgert 1996; Fadda et al. 1996). This introduces the problem of picking the best method in each situation. These methods show little differences in final results, mostly coming from borderline galaxies which do not significantly contribute to bias the cluster properties (see Wojtak et al. 2008).

In this work, we apply an initial cut-off of $\pm 3000\,\mathrm{km\,s^{-1}}$ around the cluster redshift, $z_{cl} \approx 0.042$, selecting 125 galaxies in the approximate range $9800 \lesssim V \lesssim 15\,300\,\mathrm{km\,s^{-1}}$ (see Fig. 3). Additionally, we use the shifting-gapper method (Fadda et al. 1996) to reject remaining interlopers. Here, we follow the procedure outlined by Owers et al. (2009) and Owers, Nulsen & Couch (2011). The initial step is to determine the centre of the galaxy spatial distribution. Although we have two nominal clusters in the field, we first consider that A3407 and A3408 may form a single system, at least in the velocity space, and hence we need to provide one single centre to this field. Using *ROSAT* All-Sky Survey maps, we define this centre as the peak in the X-ray emission from A3407, the richest cluster of the pair. The BCG of A3407, ESO 207-19, an object of absolute magnitude $M_R = -22.64$, is ∼51 arcsec (∼30 kpc) away from this peak, and ∼7 arcmin (∼240 kpc) away from the luminosity-weighted centroid of the distribution (see Fig. 4).

Next, galaxies are sorted into bins as a function of radial distance from the centre of the cluster. The bin size is 0.4 Mpc or larger to force the selection of at least 15 galaxies (Fadda et al. 1996; Lopes et al. 2009). Within each radial distance bin, galaxies are sorted by their peculiar velocity with respect to the velocity of the cluster. We define this peculiar velocity as

$$v^i_{pec} = c\frac{(z_i - \bar{z})}{(1+\bar{z})}, \tag{2}$$

where v^i_{pec} is the peculiar velocity of galaxy i, z_i is the redshift of galaxy i, and $\bar{z}$ is the average redshift of the cluster. In each bin, the 'f-pseudosigma' (Beers, Flynn & Gebhart 1990) is determined and used as the velocity gap to reject outliers. The value of f-pseudosigma (S_f) corresponds to the normalized difference between the upper (F_u) and lower (F_l) fourths of a data set. It can be calculated as follows:

$$S_f = \frac{(F_u - F_l)}{1.349}. \tag{3}$$

The constant 1.349 is the typical difference ($F_u - F_l$) for standard normal distributions (Beers et al. 1990). This process is repeated for each bin until either the number of sources stabilizes, the value of

[4] 6dFGS data base, http://www-wfau.roe.ac.uk/6dFGS/

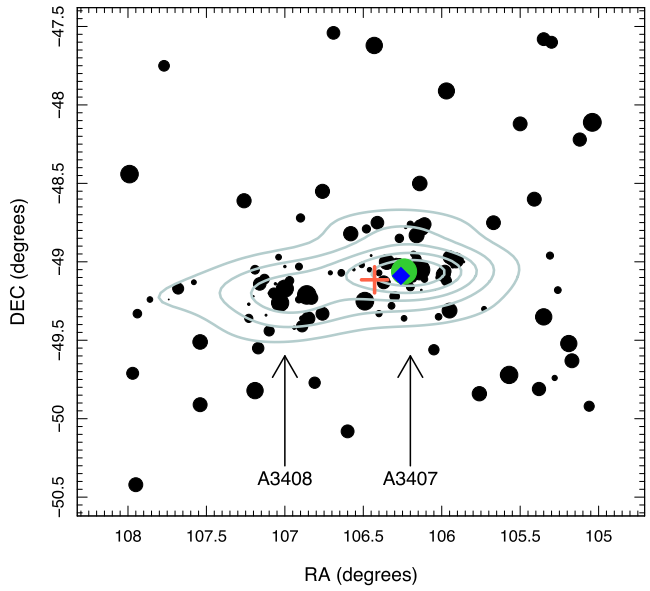

Figure 4. Galaxy distribution around A3407 and A3408. The size of each point is proportional to the galaxy luminosity. The central part of the field is outlined by the density contours. The red cross indicates the luminosity-weighted centroid of the distribution, the green filled circle indicates the BCG, and the blue diamond is the peak of the X-ray emission.

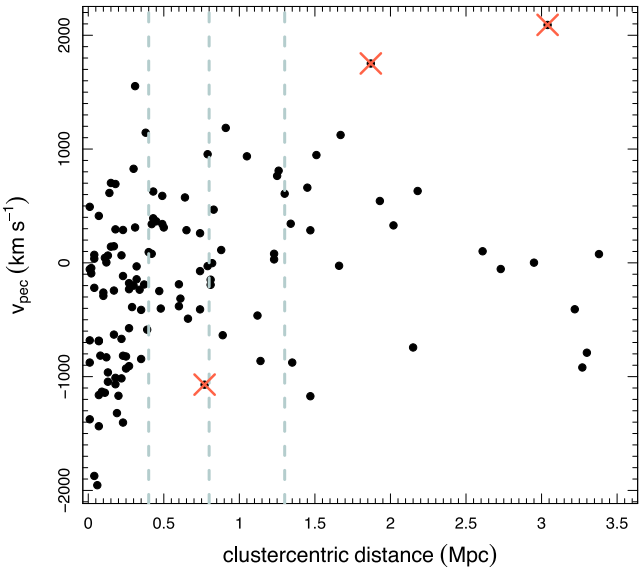

Figure 5. Galaxy clustercentric distances against the peculiar velocities with respect to the cluster velocity. The size of each point is proportional to the galaxy luminosity. The objects marked in red are those excluded by the outliers removal process. The vertical dashed lines indicate the radial bins within which galaxies were sorted by their peculiar velocity.

f-pseudosigma drops below 250 km s^{-1}, or the value of f-pseudosigma begins to increase (e.g. Wing & Blanton 2013).

After completion of the removal process, a total of 122 galaxies remained in the sample within a clustercentric radius of ∼3.5 Mpc (see Fig. 5).[5] For this data set, we determine the location (velocity mean) and scale (velocity dispersion), using the biweight estimators $C_{\rm BI}$ and $S_{\rm BI}$ (see the definitions in Beers et al. 1990). These estimators have a wide use in science since they are less sensitive to outliers and the shape of the underlying distribution (e.g. Croux & Dehon 2013). By applying the ROSTAT software (Beers et al. 1990), we find $C_{\rm BI} = 12\,415^{+110}_{-50}$ km s^{-1}, and $S_{\rm BI} = 691^{+74}_{-35}$ km s^{-1}. The errors correspond to the 68 per cent confidence interval, calculated after bootstrap re-samplings of 10 000 subsamples of the velocity data.

[5] The result of the removal process is the same as choosing the centroid or the BCG location as the centre of the system.

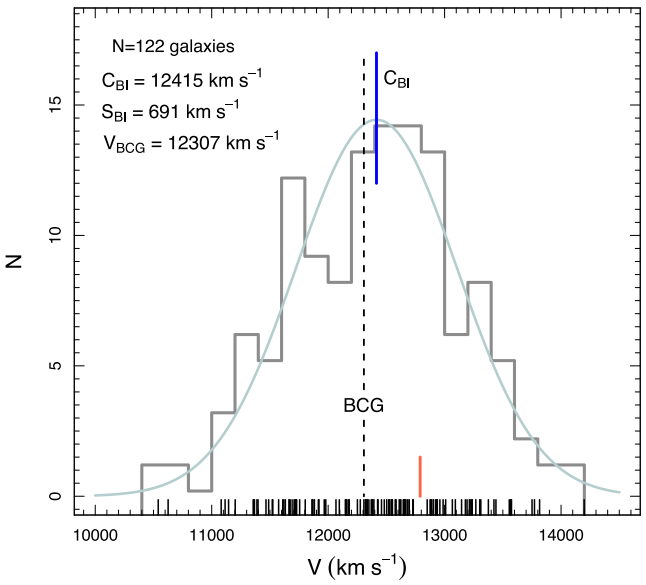

Figure 6. Velocity distribution histogram with bins of width 200 km s^{-1}. The solid line is the Gaussian with mean 12 415 km s^{-1} and standard deviation of 691 km s^{-1}. The vertical blue line indicates the mean and the dashed line indicates the BCG. At the bottom, a rug plot is shown, with the red line indicating the position of the significant weighted gap.

The velocity distribution of the clusters members is shown in Fig. 6. Also in this figure, we depict the position of the BCG galaxy, $V_{\rm BCG} = 12\,307 \pm 24$ km s^{-1}. Following Teague, Carter & Gray (1990), we test if this galaxy can be central in the A3407 + A3408 velocity field using

$$S_{\rm V} = \frac{|C_{\rm BI} - V_{\rm BCG}|}{[\delta v_{\rm cl}^2 + \delta v_{\rm BCG}^2]^{1/2}}, \quad (4)$$

where $\delta v_{\rm cl}$ and $\delta v_{\rm BCG}$ are the errors in the biweight and the BCG velocities. Values of $S_{\rm V} \gtrsim 2$ mean that the BCG peculiar motion is probably significant. For our sample, $S_{\rm V} \simeq 1.29$, indicating that we cannot reject the BCG location as being on the dynamical centre of the field (see Fig. 6). Indeed, the BCG is offset relative to the X-ray peak by only ∼30 kpc, and offset scales up to ∼50 kpc can be explained by small amplitude oscillations of the central galaxy around the bottom of the cluster potential well (see Lazzati & Chincarini 1998).

3.2 Normality

The velocity distribution of galaxies in clusters can provide information about the dynamical state of these systems. The normality of the radial velocity distribution is usually related to the dynamical equilibrium of a galaxy cluster. Both theoretical and phenomenological developments suggest that the virialized equilibrium state of a spherical gravitational system is approximately described by a Maxwell–Botzmann distribution function (Ogorodnikov 1957; Lynden-Bell 1967; Ueda, Itoh & Suto 1993; Hjorth & Williams

Table 1. Statistical tests for normality with the respective *p*-values and diagnostics at the 95 per cent confidence level.

Test	*p*-value	Diagnostics
W^2	0.276	NORMAL
U^2	0.258	NORMAL
A^2	0.414	NORMAL
KS	0.250	NORMAL
B2	0.330	NORMAL
TI	0.113	NORMAL
a	0.218	NORMAL
W	0.678	NORMAL
u	0.800	NORMAL
B1	0.278	NORMAL
AI	0.193	NORMAL

2010; Barne & Williamss 2012; Beraldo e Silva, Lima & Sodré 2013). In phase-space, this translates to a Gaussian function (or Normal distribution). *N*-body numerical experiments of the relaxation of single isolated gravitational systems (Merrall & Henriksen 2003) or that of cosmological haloes (Hansen et al. 2005; Hansen, Moore & Zemp 2006) also support these conclusions.

This suggests that discriminating groups according to their velocity distributions may be a promising way to assess the dynamics of galaxy systems. Unfortunately, this is not a simple task. Beers et al. (1990) stress the difficulty in determining when a given velocity distribution differs significantly from normality, pointing out that the classification of a cluster as Gaussian or non-Gaussian may be dependent on the statistical test used in the analysis. This suggests the need of using several complementary statistical tests to achieve a reliable diagnostic (Beers et al. 1990; Bird & Beers 1993; Ricker & Sarazin 2001; Hou et al. 2009; Ribeiro et al. 2013).

We can distinguish three categories of normality tests among those included in the ROSTAT package. The omnibus tests, which try to quantify the overall deviation of the velocity distribution from a Gaussian, such as the Cramer von-Mises W^2 test, the Watson U^2 test, the Anderson–Darling A^2 test, and the Kolmogorof–Smirnov (KS) test (see Beers, Gebhart & forman 1991, for references). The shape tests, which are devised to measure the shape of the outskirts of the distribution, such as the kurtosis test (the B2 test) and its robust counterpart, the Tail Index test (see Bird & Beers 1993, for a discussion), or to test its tail population, such as the a and the W tests, which are most sensitive to the tail of the underlying populations, and the u test, which is sensitive to contamination by extreme values (see Yahil & Vidal 1977, for a discussion on these tests). Finally, there are tests which measure the asymmetry of the distribution: the skewness test (B1 test) and its robust version, the Asymmetry Index (AI) test (Bird & Beers 1993). For each of these tests, ROSTAT computes its statistics as well as their associated *p*-values (Beers et al. 1990). In Table 1, we present the results of all these tests, which unanimously failed to reject he normality of the velocity distribution of the A3407 + A3408 field.

3.3 Unimodality

Although the tests used in the previous section consistently indicate normality, we explore the possibility of gaps in the velocity distribution. The ROSTAT package provides two statistical tests helping to identify kinematical features in the velocity distribution. These are the gap analysis (Wainer & Shacht 1978) and the dip unimodality test (Hartigan & Hartigan 1985). The dip test measures the maximum difference, over all sample points, between the empirical distribution function, and the unimodal distribution function. Since the dip statistic is asymptotically larger for the uniform than for any distribution in a wide class of unimodal distributions, it appears to be a reasonable measure of the extent of deviation from unimodality (Hartigan & Hartigan 1985). The gap analysis estimates the probability that a gap of a given size and location, between the ordered velocities, may be produced by random sampling from a Gaussian population. First, the velocities are sorted in increasing order and the *i*th velocity gap is given by $g_i = v_{i+1} - v_i$. The weight for the *i*th gap is $w_i = i(N-i)$ and the weighted gap is defined as $\sqrt{w_i g_i}$. The weighted gaps are normalized through dividing by the mid-mean (MM) of the ordered weighted gap distribution given by

$$\mathrm{MM} = \frac{2}{N} \sum_{i=N/4}^{3N/4} \sqrt{w_i g_i}. \tag{5}$$

We look for normalized gaps larger than 2.25, since in random draws of a Gaussian distribution, they arise at most in ∼3 per cent of the cases (see Wainer & Shacht 1978; Beers et al. 1991). We detect one significant gap at $V \simeq 12\,790$ km s^{-1} (see Fig. 6). This could be an indication that the distribution is bimodal. However, normality was not rejected after a battery of tests, and the dip test also failed to reject the unimodality with p-value = 0.7542. To explore a little more this result, we test if our sample can be model as a normal mixture using the MCLUST code (Fraley & Raftery 2006). MCLUST is a contributed R package, an open-source free statistical environment developed under the GNU GPL (Ihaka & Gentleman 1996, http://www.r-project.org). The method is based on a search of an optimal model for the clustering of the data among models with varying shape, orientation and volume. It finds the optimal number of components and the corresponding classification (the membership of each component). We run MCLUST on 10 000 bootstrap re-samplings of the velocity data and on 10 000 realizations of a normal distribution with $\mu = C_{\rm BI}$ and $\sigma = S_{\rm BI}$. We find bimodality in 13 per cent of times for the re-samplings of the observed distribution, and 11 per cent of times for the normal realizations. The closeness of these values suggests a situation where bimodality may be undetectable to MCLUST and other statistical tests. We should recall that not all mixture of two unimodal distributions with differing means is necessarily bimodal. For instance, the Holzmann & Vollmer (2008) bimodality indicator, given by

$$d = \frac{|\mu_1 - \mu_2|}{2\sqrt{\sigma_1 \sigma_2}}, \tag{6}$$

indicates that a mixture should be considered bimodal only if $d > 1$. For the A3407+A3408 velocity field, the mixture detected with MCLUST has the following parameters: $\mu_1 \simeq 11\,979$ km s^{-1}, $\sigma_1 \simeq 596$ km s^{-1}, $\mu_2 \simeq 12\,826$ km s^{-1}, and $\sigma_1 \simeq 527$ km s^{-1}, which leads to $d = 0.75$, and thus we cannot reject unimodality.

3.4 Velocity gradient

Up to this stage, we found that the velocity distribution of the A3407+A3408 field is consistent with both unimodality and normality. Also, the BCG galaxy does not have a significant peculiar motion with respect to the centre of the velocity distribution. Now, we want to consider a further question: can the gap identified in the velocity distribution be indicating a velocity gradient across the spatial galaxy distribution? To explore this possibility, we estimate the principal axis of the galaxy projected distribution using the moments of inertia method (Carter & Metcalfe 1980). From the eigenvectors of the spatial configuration, we find the direction of the

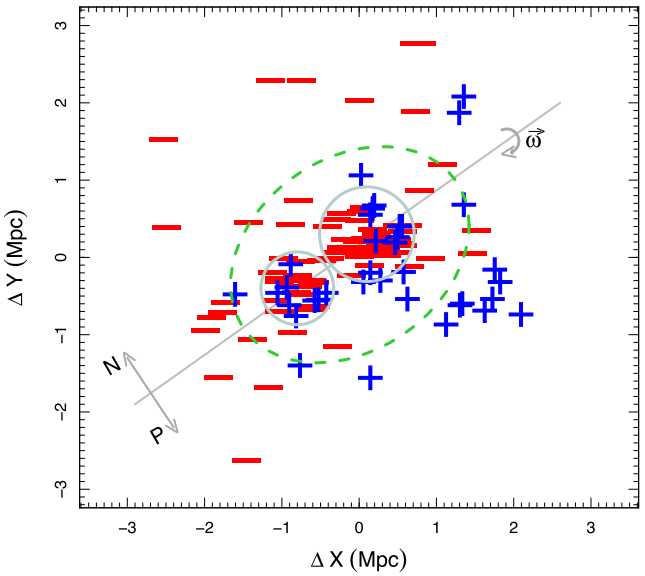

Figure 7. Distributions of galaxies projected on the sky plane. The symbols '+' and '−' indicate positive or negative velocity with respect to the gap position. The vector $\vec{\omega}$ indicates the possible rotation around the principal axis. Directions used for distance summations are given by 'N' (negative) and 'P' (positive). The dashed green ellipse indicates the region containing 90 per cent of data. The circles indicate the approximate regions of A3407 and A3408.

principal axis of the system, as shown in Fig. 7. Next, we divide the sample in two groups, above or below the gap position, and compute the perpendicular distance of each object to the principal axis. We adopt arbitrary signs for the distances on each side of the axis (see Fig. 7). Let us call S1 and S2 the total sum of distances for objects in group 1 ($V < 12\,790$ km s^{-1} and 86 galaxies) and in group 2 ($V > 12\,790$ km s^{-1} and 36 galaxies). We find S1 $= -11.92$ Mpc and S2 $= 14.60$ Mpc, respectively. The significance of this result is determined by running 10 000 realizations of two spatial Poisson processes with the same number of points as groups 1 and 2, and within the same limits of the real galaxy distribution: $[-3, 3] \times [-3, 3]$ Mpc. Distances of all points to the principal axis are computed and summed just as we did before. At the end of the runs, we have an output distribution reflecting the possible range of sums. To achieve a result indicating a significant velocity gradient, at least one of the sums observed (S1 or S2) must be outside the robust 95 per cent confidence level interval, which are I1: $[-12.53, 19.86]$ Mpc and I2: $[-10.32, 13.05]$ Mpc (for Poisson processes with 86 and 36 points, respectively). Hence, while S1 is consistent with I1, S2 is more positive than I2, suggesting the possibility of an asymmetric velocity distribution across the spatial distribution, i.e. high-velocity galaxies may be segregated spatially with respect the principal axis. This velocity gradient of $\sim 847 \pm 114$ km s^{-1} could indicate some rotation $\vec{\omega}$ around this axis (see Fig. 7). It is consistent with typical gradients ($240 - 1230$ km s^{-1}) found in clusters studied by den Hartog & Katgert (1996).

A galaxy system can acquire angular momentum from cosmological ab initio conditions from their formation times (Li 1998; Liao et al. 2015). Another possibility is through an off-axis merging between two clusters (Ricker 1998; Takizawa 2000; Pawl, Evrard & Dupke 2005). This does not seem to be the case of A3407 and A3408, since they both are well aligned with the cluster principal axis (see Fig. 7). It should also be noted in this figure that the two velocity components (the positive and negative values with respect to the gap) are widespread in the field, permeating both A3407 and A3408. That is, the velocity gradient is not reflecting only the central structures in the field. This could mean that the galaxy distribution in and around A3407 and A3408 may have acquired this pattern in the same cosmic event, whose nature is not clear at the moment.

Finally, it is worth noting that a rotating system does not mean a non-equilibrium system. In fact, Hwang & Lee (2007) studied two probable rotating clusters (Abell 954 and Abell 1399) and verified that they may be in dynamical equilibrium and have undergone no recent merging. Similarly, Oegerle & Hill (1992) found that the highly probable rotating cluster Abell 2107 has galaxy velocities consistent with a Gaussian distribution.

Table 2. Statistical tests for substructures with the respective p-values and diagnostics at the 95 per cent confidence level.

Test	p-value	Diagnostics
β	0.001	SUBSTRUCTURES
Δ	0.028	SUBSTRUCTURES
Lee 2D	0.002	SUBSTRUCTURES
Lee 3D	0.016	SUBSTRUCTURES

4 SUBCLUSTERING

Although the A3407+A3408 field can be described by a single Gaussian velocity distribution, we cannot say they constitute a single dynamical unit without taking into account their spatial coordinates. To examine this more general situation, we consider once more that A3407 and A3408 may form a single cluster – the hypothesis to be tested. Then, we apply statistical tests to check if A3407 and A3408 emerge as independent entities.

A cluster is said to contain substructures (or subclusters) when its surface density is characterized by multiple, statistically significant peaks, in combination with the distribution of galaxy velocities (e.g. Ramella et al. 2007). A variety of statistical tests are available to assess the presence of substructures in galaxy clusters (see Pinkney et al. 1996; Biviano et al. 2006). We chose to apply four of them: The β test (West, Oemler & Dekel 1988), the Δ test (Dressler & Shectman 1988), and the Lee 2D and 3D statistics (Lee 1979; Fichett & Webster 1987), conducted here following the work of Pinkney et al. (1996). They can be briefly described as follows.

(i) The β statistics is a 2D estimator of deviations from the mirror symmetry about the cluster centre.
(ii) The Δ statistics evaluates the kinematics of galaxy groups identified in sky projected clusters.
(iii) The Lee 2D statistics is a measure of the clumpiness in the locations of galaxies after they have been projected on to a line.
(iv) The Lee 3D statistics extends the procedure to include a third 'dimension' given by velocity data.

Results presented in Table 2 indicate the presence of subclusters in the field. To separate them, we take the full available phase-space information making use of the KMM algorithm (Ashman, Bird & Zepf 1994), applied to the distribution of cluster members in the 3D-space of positions and velocities. We search for the solution that separates the members into two subclusters. The KMM algorithm uses the maximum-likelihood ratio test to estimate how likely the two-system solution is to be a significant improvement over the single-system solution (e.g. Barrena et al. 2002).

We find that the solution with two subclusters is significantly better than the single unit solution, at the 99 per cent confidence level.

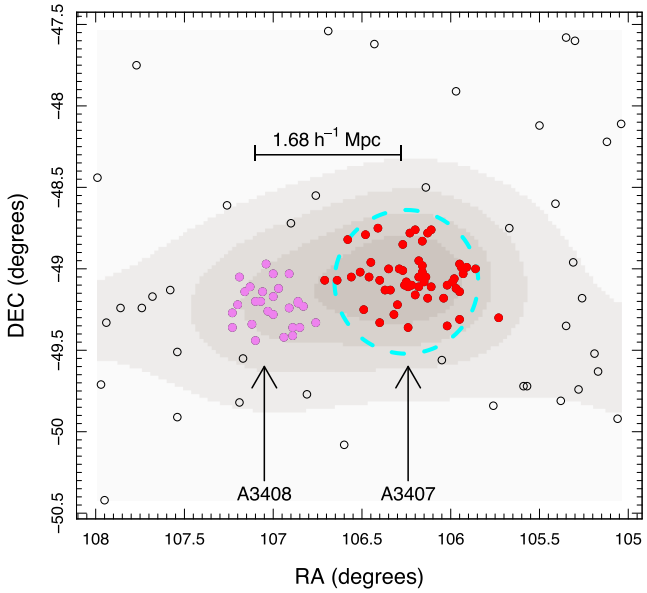

Figure 8. Two subclusters, corresponding to A3407 and A3408, identified by the KMM algorithm. Densities are depicted by grey shades. A3407 and A3408 are indicated in red and purple colours. The cyan circle encompasses the region whose density is 2σ higher than the average.

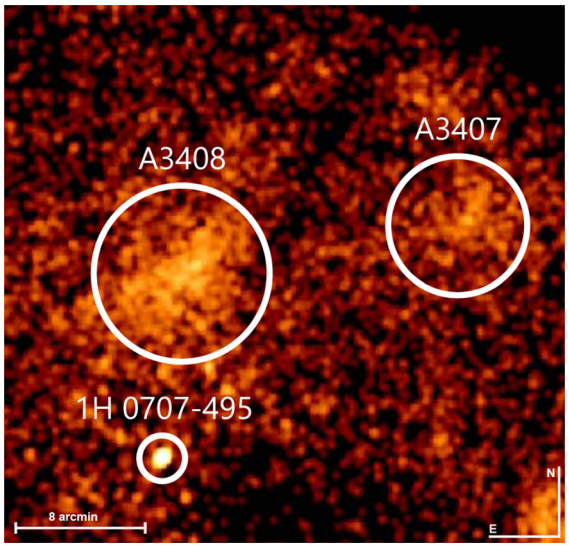

Figure 9. *ROSAT* PSPC smoothed (with a 3 arcsec width Gaussian) image from a pointed 9.5 ksec observation RP180306N00. Also shown the AGN 1H 0707-495, the main target of that observation. The circles surrounding A3408 and A3407 have 10 and 8 arcmin radii and illustrate the X-ray emission of the A3407–A3408 pair.

In Fig. 8, we show the two subclusters identified. Not surprisingly, they correspond to A3407 and A3408, individually identified for the first time in this work. In this figure, we also indicate the circle containing the region whose density is 2σ higher than the average of the full sample (let us call it $R_{2\sigma}$, with $R_{2\sigma} = 0.88\,\mathrm{h}^{-1}$ Mpc). This circle completely encompasses the main system (A3407), and leaves the secondary system (A3408) completely outside $R_{2\sigma}$. KMM assigns 27 galaxies to A3408, each at the 99 per cent cl. From these galaxies, we compute the mean velocity $V_{\mathrm{A3408}} = 12\,458 \pm 98$ km s^{-1} and velocity dispersion $\sigma_{\mathrm{A3408}} = 573^{+48}_{-37}$ km s^{-1}. At the same time, KMM assigns 54 galaxies to A3407, each at the 99 per cent cl. The resulting mean velocity is $V_{\mathrm{A3407}} = 12\,328 \pm 116$ km s^{-1} with velocity dispersion $\sigma_{\mathrm{A3407}} = 718^{+61}_{-42}$ km s^{-1}. The projected distance between the X-ray peaks of each cluster is $1.68\,\mathrm{h}^{-1}$ Mpc. This distance extends beyond $R_{2\sigma}$, suggesting a significant physical separation between the clumps. On the other hand, the relative velocity between the two systems is not significant in comparison with the errors, $\Delta V = 130 \pm 151$ km s^{-1}. This small velocity separation is consistent with our previous findings on normality and unimodality, suggesting the existence of a single cluster in the velocity space. However, the double peak in the galaxy spatial distribution is also present in the X-ray emission, as we can see in the *ROSAT* All-Sky Survey image – Fig. 9. In this figure, we also see that there is no common X-ray halo in the field, which weakens the idea of a single dynamical unit for A3407 + A3408. From now on, we assume that A3407 and A3408 are individual systems.

5 DYNAMICAL ANALYSIS

5.1 Virial mass

Before obtaining the virial mass of each individual cluster, we need to check whether their velocity distributions are Gaussian. If that is the case, we can assume virialization. Applying the same statistical tools used in Section 3.2, we verified that none of them rejects normality of the velocity distributions of A3407 and A3408 at the 95 per cent cl. (with p-values ≥ 0.116 and 0.347, respectively). Another virialization indicator is the crossing-time of a galaxy system. According to Nolthenius & White (1987), a system with crossing-time $> 0.09\ \mathrm{H}_0^{-1}$ (hereafter $t_{\mathrm{c}}^{\mathrm{vir}}$) probably has not yet had time to virialize. The crossing-time is calculated as

$$t_{\mathrm{c}} = \frac{3 r_{\mathrm{H}}}{5^{3/2}\sigma_{\mathrm{v}}}, \tag{7}$$

(Huchra & Geller 1982), where the harmonic radius, r_{H}, is independent of the velocity dispersion and is given below:

$$r_H = \pi D \sin\left[\frac{n(n-1)}{4\sum_i \sum_{j>i} \theta_{ij}^{-1}}\right], \tag{8}$$

where D is the distance to the group, n is the number of members of each group, and θ_{ij}^{-1} is the angular separation of group members. Setting up the cosmological parameters as $\Omega_{\mathrm{M}} = 0.3$ and $\Omega_{\Lambda} = 0.7$, we find the distances to each system: 122.14 h^{-1} Mpc (A3407) and 123.40 h^{-1} Mpc (A3408), that leads us to $t_{\mathrm{c}} = 0.041\ \mathrm{H}_0^{-1}$ (A3407) and $t_{\mathrm{c}} = 0.037\ \mathrm{H}_0^{-1}$ (A3408), which is a further indication that these systems are virialized. In the same way, the crossing-time for the whole A3407+A3408 cluster is $t_{\mathrm{c}} = 0.053\ \mathrm{H}_0^{-1}$, also a lower value than $t_{\mathrm{c}}^{\mathrm{vir}}$, indicating that even this larger system has had time to virialize.

Assuming from now on that the virial theorem applies, the system is self-gravitating, and the bodies in the system have equal masses, the virial mass estimator is usually written as

$$M_V = \frac{3\pi N}{2\,G}\frac{\sum (v_i - V)^2}{\sum_{i<j} 1/R_{ij}}, \tag{9}$$

where N is the number of cluster members, v_i is the velocity of the ith galaxy, V is the mean of all members, and R_{ij} is the projected separation between the two galaxies i and j (Heisler, Tremaine & Bahcall 1985). We summarize all the structural and dynamical properties in Table 3. Errors on r_H and σ were calculated using the bootstrap method for 10 000 re-samplings and then used standard

Table 3. Structural and dynamical properties of clusters A3407 and A3408.

Cluster	σ (km s^{-1})	r_H (h^{-1} Mpc)	log M_V (h^{-1} M$_\odot$)	t_c (H_0^{-1})
A3407	718^{+93}_{-48}	$1.10^{+0.12}_{-0.13}$	$14.59^{+0.46}_{-0.42}$	$0.041^{+0.011}_{-0.009}$
A3408	573^{+82}_{-59}	$0.80^{+0.21}_{-0.13}$	$14.26^{+0.55}_{-0.46}$	$0.037^{+0.010}_{-0.009}$
A3407+08	691^{+74}_{-35}	$1.36^{+0.27}_{-0.18}$	$14.66^{+0.64}_{-0.57}$	$0.053^{+0.012}_{-0.012}$

error propagation analysis to calculate the rms error on the crossing-time and the virial mass.

5.2 Two-body model

The stage is being set for a possible merger of A3407 and A3408. By knowing their virial masses and the spatial separation, we can use the Newtonian binding criterion that a two-body system is bound if the potential energy of the bound system is equal to or greater than the kinetic energy. To assess the likelihood that A3407 and A3408 are bound to one another, we require

$$V_r \leq \left(\frac{2GM_{tot}}{R_p}\right)^{1/2} (\cos\alpha)^{1/2} \sin\alpha, \quad (10)$$

where $V_r = V \sin\alpha$, $R_p = R\cos\alpha$, M_{tot} is the combined mass of the two bodies, and R and V are true (3D) positional and velocity separation between the two objects. V_r is line-of-sight relative velocity between the two bodies and R_p is the projected separation, and α is the projection angle between the plane of the sky and the line that joins the centres of the two objects (Beers, Geller & Huchra 1982; Gregory & Thompson 1984; Cortese, Gavazzi & Boselli 2004; Brough, Forbes & Kilborn 2006). This model assumes radial orbits for the clumps, which are assumed to start their evolution at time $t_0 = 0$ with separation $R_0 = 0$, and are moving apart or coming together for the first time in their history, i.e. we are assuming that we are seeing the cluster prior to merging. The only quantity to be determined in equation (10) is α. We must probe the $V_r - \alpha$ space to define the probability that the system is gravitationally bound for a given projection angle. That probability can be calculate from

$$P_{bound} = \int_{\alpha_1}^{\alpha_2} \cos\alpha \, d\alpha \quad (11)$$

(Girardi et al. 2005). Using the parameters previously found, $R_p = 1.68\,h^{-1}$ Mpc, $V_r = 130$ km s^{-1}, $M_{tot} = 4.53\,h^{-1} \times 10^{14}$ M$_\odot$, and taking 9.03 h^{-1} Gyr, as the age of the Universe at $z \approx 0.042$, we can solve the two-body problem. The solutions are shown in Fig. 10, where the dashed line depicts the bound-outgoing solution (BO) and the solid black line depicts the bound-incoming solution (BI). There are two solutions in the BI case (BI$_a$ and BI$_b$) due to the ambiguity in the projection angle α. All the solutions are defined by the vertical blue line corresponding to the relative velocity with the shaded area associated with the error ± 151 km s^{-1}. The red line in Fig. 10 separates the bound and unbound regions according to the Newtonian criterion. The general result is that the A3407 and A3408 are likely to be bound at the 84 per cent level.

The two-body model has three solutions: two collapsing or ingoing and one expanding or outgoing. Considering the angle of parametrization χ obtained from the spherical collapse model (between $0 < \chi < 2\pi$), we can describe the temporal evolution and the different relative positions of the binary system (Peebles 1993).

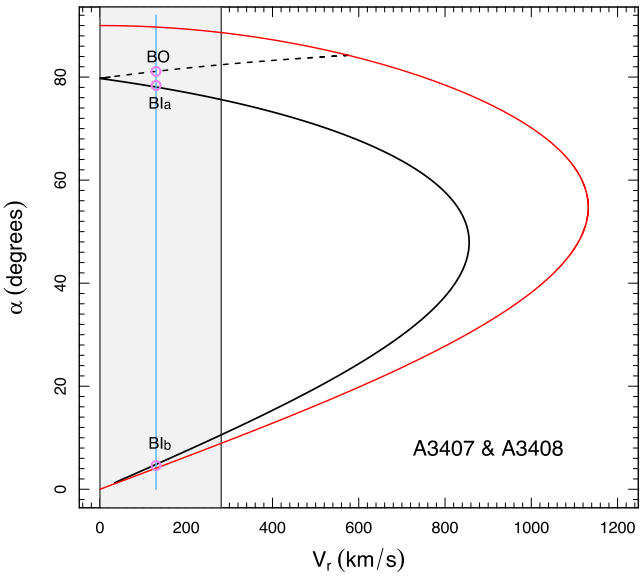

Figure 10. Orbits in the two-body model as a function of α, the projection angle of A3407 and A3408, and V_r, the radial velocity. The vertical blue line represents the relative radial velocity $V_r = 130 \pm 151$ km s^{-1}, with the shaded area indicating the respective uncertainty. The solid curve depicts the bound-incoming solution while the dashed one depicts the bound-outgoing solution. The red line separates the bound and unbound regions according to the Newtonian criterion.

Table 4. Solutions of the two-body model for A3407 and A3408.

Sol.	α (○)	V (km s^{-1})	R (h^{-1} Mpc)	R_m (h^{-1} Mpc)	t h^{-1} Gyr
BO	73.25	140.83	4.45	4.56	5.38
BI$_a$	67.85	− 135.68	5.83	6.00	3.56
BI$_b$	6.67	− 1080.85	1.69	3.43	8.23

These solutions allow us to estimate the time-scale for the system to reach the maximum expansion. Using the equations of motion:

$$t = \left(\frac{R_m^3}{8GM}\right)^{1/2} (\chi - \sin\chi), \quad (12)$$

$$R = \frac{R_m}{2}(1 - \cos\chi), \quad (13)$$

$$V = \left(\frac{2GM}{R_m}\right)^{1/2} \frac{\sin\chi}{(1-\cos\chi)}, \quad (14)$$

where R is the separation at time t, R_m is the separation at the maximum expansion, and V is the relative velocity. We can solve this system of equations for V_r and α using equation (6) from Gregory & Thompson (1984):

$$\tan\alpha = \left(\frac{tV_r}{R_p}\right) \frac{(\cos\chi - 1)^2}{\sin\chi(\chi - \sin\chi)}. \quad (15)$$

In Table 4, we present the parameters of the two-body model solutions. In solution BO, the system is initially 4.45 h^{-1} Mpc apart, and would still take $\sim$0.76 h^{-1} Gyr to reach the maximum expansion. In solution BI$_a$, the system is 5.83 h^{-1} Mpc apart with a low colliding velocity of 135.68 km s^{-1}. In these two first solutions, the cluster cores will cross each other after a long time ($\geq$10 Gyr). The only solution consistent with a close encounter is the BI$_b$ solution, where clusters are close together with a high colliding velocity of

1080.85 km s^{-1}, and the cluster cores will cross in less than $\sim 1\,h^{-1}$ Gyr. Thus, while the BO and BI$_a$ solutions do not predict strong interactions between A3407 and A3408, the BI$_b$ solution allows a more intense dynamics for this pair. This latter possibility is examined in Section 6.

5.3 Caveats about the method

Before proceeding, we have to recognize some weaknesses of the two-body model. First of all, we should keep in mind that the two-body model does not consider the angular moment of the system, which is unlikely to be zero, since we have identified a velocity assymetry around the principal axis of the galaxy projected distribution, suggesting a rotating object. The reason this could be important to any dynamical analysis is that the corrected cluster mass can be reduced by ∼20 per cent–30 per cent, on average, with respect to that uncorrected for rotation, as shown in Manolopoulou & Plionis (2016). An additional weakness of the two-body model is not considering the distribution of matter inside each cluster. As clusters merge, their haloes overlap and dark matter constraints should be taken into account, as shown in Nusser (2008). Finally, we also ignored the gravitational interaction of the infalling matter outside the cluster pair, which could affect the assumption that masses are constant since their formation time (Angus & McGaugh 2008). All these points may modify the results presented in Section 5.2.

6 DISCUSSION

It is not easy to distinguish the most reasonable two-body dynamical solution. Several other factors must be considered to come up with a viable physical scenario. In this work, the solution that can be best assessed with the available data is BI$_b$, in which the close proximity of the clusters combined with the high colliding velocity would suggest that the system is about to coalesce, and should already be experiencing some dynamical interactions. If the system was at such evolutionary state, we would expect to see some disturbances in the velocity distributions, which has not been observed in this work: both clusters have Gaussian velocity distributions (see Section 5.1). In addition, applying the statistical tests described in Section 4, none of them indicates the presence of substructures in A3408 at the 95 per cent cl. (with p-values > 0.221), and only the DS test indicates substructures in A3407 at the 95 per cent cl. (p-value = 0.016). Hence, these results (taken separately) are not indicating strong dynamical interactions in the pair.

But cluster dynamics is also related to galaxy evolution. A cluster–cluster interaction may affect galaxy orbits, star formation rates, colours, and morphologies. From this perspective, there are some important differences between A3407 and A3408. A3407 has a higher fraction of emission line galaxies, ∼30 per cent, in comparison to A3408, ∼8 per cent. Also, galaxies in A3408 are redder [$\langle B-R\rangle = 1.83 \pm 0.22$] than in A3407 [$\langle B-R\rangle = 1.47 \pm 0.12$], with the KS test indicating colour distributions significantly different between the clusters (p-value $< 10^{-4}$). Finally, while the BCG in A3407 has larger magnitude differences with respect to the second and third brightest galaxies [$\Delta m_{12} = 0.62$, $\Delta m_{13} = 0.75$], in A3408, basically, there is no magnitude difference between the three first ranked galaxies [$\Delta m_{12} = 0.01$, $\Delta m_{13} = 0.01$]. These findings are further examples of the complexity of this pair. A3408 seems to contain more evolved galaxies with significant suppression of the star formation rate. At the same time, this cluster does not have an unquestioned BCG (three galaxies could take the position). This is not in agreement with the central galaxy paradigm, which states

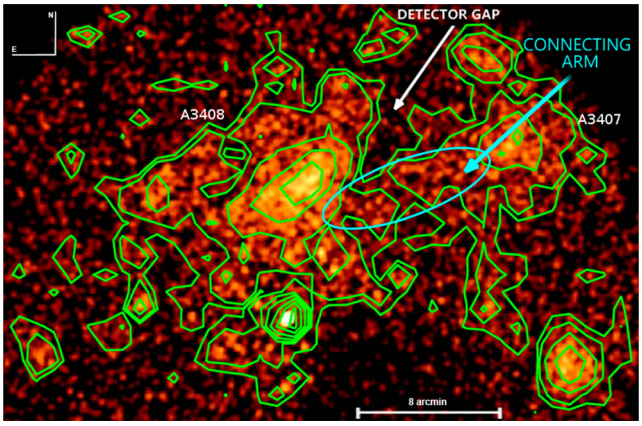

Figure 11. X-ray emission around A3407 and A3408 with isophotes in green. A possible 'arm' connecting the clusters is highlighted. *ROSAT* image.

that a BCG, with pronounced luminosity gap, should be at rest at the centre of the cluster. The amplitude of the luminosity gap is a function of the formation epoch, the halo concentration, and the recent infall history of the cluster (see Smith et al. 2010). This could be suggesting a dark matter halo less concentrated or disturbed in A3408. Disturbances in DM correspond well to what we expect from the BI$_b$ solution, and would probably leave traces in the X-ray emission.

Taking a closer look at the X-ray distribution around A3407 and A3408, we note a complex and patchy X-ray morphology extended in the SE-NW direction of this field – Fig. 11. In A3407, the *ROSAT* image suggests the presence of substructures, and the cluster core shows an elongation roughly in the same direction as that of A3408. In A3408, the X-ray diffuse emission has an elongation SE-NW (not towards A3407, but with similar elongation direction of its core). We also should note in this figure a weak bridge or 'arm' leaving A3407 and going towards A3408. Since this arm does not seem to be the result of point sources, it may indicate the existence of a physical connection between the clusters. These X-ray features are compelling indicators of dynamical interactions between A3407 and A3408, and suggest the BI$_b$ solution as a viable model for the pair. Indeed, the X-ray emission around this field could be also consistent with a merger having happened in the SE-NW direction, which is approximately coincident with the principal axis of the galaxy projected distribution (see Section 3.4). If that is the case, we may be witnessing a major post merging event. Indeed, from the X-ray temperature, Katayama et al. (2001) find $\sigma = 674 \pm 23$ km s^{-1}, significantly higher than the velocity dispersion we found from galaxies, $\sigma = 573^{+82}_{-59}$ km s^{-1}. This could mean that the gas temperature may be enhanced by previous-ongoing shock heating due to a merger. Running the two-body model for $2\pi < \chi < 4\pi$, we find two expanding (outgoing) solutions with low (174 km s^{-1}) and high velocities (1135 km s^{-1}), and probability of being a gravitationally bound system of ∼8 per cent, with cores having crossed each other $\sim 1.65\,h^{-1}$ Gyr ago.

The post-merger scenario can be further explored with the Dawson's method – the Monte Carlo Merger Analysis Code (MCMAC).[6] The method takes observed priors on each cluster's mass, radial velocity, and projected separation, draws randomly from those priors, and uses them in an analytic model to get posterior Probability Distribution Functions (PDF's) for merger dynamic

[6] A PYTHON code openly available at git://github.com/MCTwo/MCMAC.git.

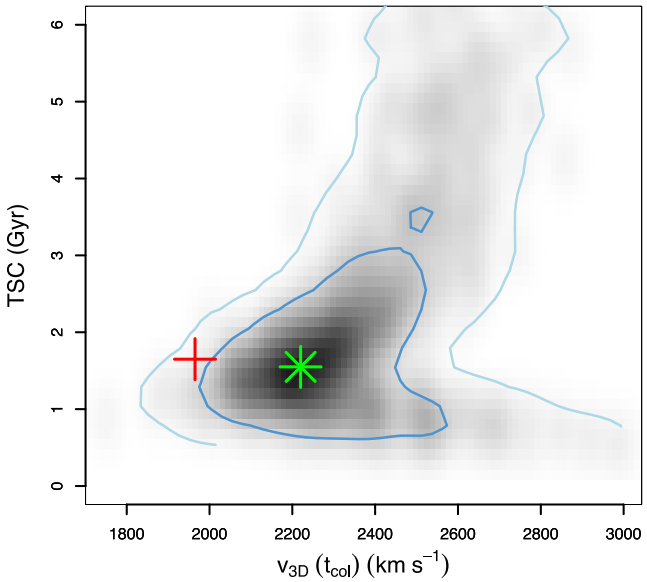

Figure 12. The posterior PDF of the A3407 and A3408 pair for the TSC and $v_{3D}(t_{col})$ parameters is shown in grey scale, with dark and light blue contours representing 68 per cent and 95 per cent confidence levels, respectively. The red cross indicates the approximate location of the traditional two-body model solution. The green star indicates the most probable solution of the MCMAC code for 10 000 realizations.

properties of interest (see Dawson 2013). This method can obtain a valid solution near the collision state, fully estimate the covariance matrix for the merger parameters, and it is in better than 10 per cent agreement with *N*-body simulations of dissociative mergers. A further advantage of the MCMAC method is that the potential gravitational energy of the pair is approximated by two truncated Navarro Frenk White (NFW) haloes, a more realistic setup for interacting clusters (Dawson 2013). Performing the analysis for A3407 and A3408 with 10 000 Monte Carlo realizations, we find the posterior distribution of the time since collision (TSC) and the 3D relative velocity $v_{3D}(t_{col})$ parameters. In Fig. 12, we see the posterior PDF of the A3407 and A3408 pair. Note that the distribution encompasses the two-body model high-velocity solution (the red cross). Here, we assume velocity isotropy and transform the line-of-sight relative velocity to the 3D one at the collision time just by multiplying a $\sqrt{3}$ factor. This allows a direct comparison with the MCMAC results. Note in Fig. 12 that the most probable solution of the MCMAC method has a higher velocity at the collision time (2220 km s^{-1}) and a similar TSC (1.55 h^{-1} Gyr) (the green star). Also, note that a low-velocity solution seems to be discarded by the MCMAC method. This result reinforces the possibility of a high-velocity post-merger solution for A3407 and A3408.

7 CONCLUSION

We performed a dynamical study of the galaxy cluster pair A3407 and A3408 based on a spectroscopic survey obtained with the 4 metre Blanco telescope at the CTIO, plus 6dF data, and also considering X-ray data from the *ROSAT* All-Sky Survey. Our main goal was to probe the galaxy dynamics in this field and verify if the sample constitutes a single galaxy system or corresponds to an ongoing merging process. The currently pair description considerably enhances the knowledge about this field, which were previously restricted to the 1990 s analyses.

As a central result, the KMM analysis and the X-ray distribution do not support the supposition made by Galli et al. (1993) that A3407 and A3408 may form a single system. Despite the very regular configuration in the velocity space, our data are consistent with two distinct objects. At the same time, redder galaxy colours and the absence of a unique BCG in A3408 indicates this system could be disturbed, in agreement with the complex X-ray distribution in this field. Signs of dynamical interactions suggest that the systems may be consistent with the fast collapsing solution of the two-body model, configuring a pre-merger scenario. In this scenario, the cluster cores will cross each other in less than $\sim 1\,h^{-1}$ Gyr. On the other hand, the gas temperature and galaxy evolution indicators in A3408 may be suggesting a post-merger scenario, with cores having crossed each other $\sim 1.65\,h^{-1}$ Gyr ago. This result is reinforced by the MCMAC analysis which provides the most probable solution (at the $\sim$82 per cent level) for the post-merger picture with TSC = 1.55 h^{-1} Gyr and $v_{3D}(t_{col}) = 2200$ km s^{-1}. Hence, that possibility cannot be rejected in this work. Further observations and *N*-body numerical simulations are required to confirm or refute each scenario discussed in this paper.

ACKNOWLEDGEMENTS

We thank the referee for relevant suggestions. We are grateful to E. Cypriano, R. Monteiro-Oliveira and G. Lima Neto for useful suggestions and discussions. We also thank the financial support of FAPESB under grant 0239/2010. ALBR and HP would like to thank the financial support from the project Casadinho PROCAD – CNPq/CAPES number 552236/2011-0. ALBR also thanks the support of CNPq, grant 309255/2013-9. MT acknowledges financial support from FAPESP (process 2012/05142-5) and CNPq (process 204870/2014-3). Finally, we would like to thank the CTIO staff.

REFERENCES

Abell G. O., Corwin H. G., Olowin R. P., 1989, ApJS, 70, 1
Allen S. W., Evrard A. E., Mantz A. B., 2011, ARA&A, 49, 409
Angus G. W., McGaugh S. S., 2008, MNRAS, 383, 417
Araya-Melo P. A., Reisenegger A., Meza A., van de Weygaert R., Dünner R., Quintana H., 2009, MNRAS, 399, 97
Ashman K. M., Bird C. M., Zepf S. E., 1994, AJ, 108, 2348
Barden S. C., Ingerson T. E., 1998, in Arribas S., Mediavilla E., Watson F., eds, ASP Conf. Ser. Vol. 152, Fiber Optics in Astronomy III. Astron. Soc. Pac., San Francisco, p. 60
Barnes E. I., Williams L. L. R., 2012, ApJ, 748, 144
Barrena R., Biviano A., Ramella M., Falco E. E., Seitz S., 2002, A&A, 386, 816
Beers T C., Gebhardt K., Forman W., 1991, AJ, 102, 1581
Beers T. C., Geller M. J., Huchra J. P., 1982, ApJ, 257, 23
Beers T. C., Flynn K., Gebhardt K., 1990, AJ, 100, 32
Beraldo e Silva L., Lima M., Sodré L., 2013, MNRAS, 436, 2616
Bertin E., Arnouts S., 1996, A&AS, 317, 393
Bird C. M., Beers T. C., 1993, AJ, 105, 1596
Biviano A., Murante G., Borgani S., Diaferio A., Dolag K., Girardi M., 2006, A&A, 456, 23
Brough S., Forbes D. A., Kilborn V. A., 2006, MNRAS, 369, 1351
Campusano L. E., Hardy E., 1996, in Kochanek C. S., Hewitt J. N., eds, Proc. IAU Symp. 173, Astrophysical Applications of Gravitational Lensing. Kluwer, Dordrecht, p. 125
Campusano L. E., Kneib J. P., Hardy E., 1998, ApJ, 496, L79
Carrasco E. R., Mendes de Oliveira C., Infante L., 2006, AJ, 132, 1796
Carter D., Metcalfe N., 1980, MNRAS, 190, 325
Cattaneo A., Mamon G. A., Warnick K., 2011, A&A, 533, A5
Clowe D., Bradac M., Gonzalez A. H., 2006, ApJ, 648, L109

Cohn J. D., White M., 2005, Astropart. Phys., 24, 316
Cortese L., Gavazzi G., Boselli A., 2004, A&A, 425, 429
Croux C., Dehon C., 2013, Robust estimation of location and scale. Encyclopedia of Environmetrics, John Wiley & Sons, Ltd., p. 5
Cypriano E. S., Sodré L., Jr, Campusano L. E., Kneib J.-P., Giovanelli R., Haynes M. P., Dale D. A., Hardy E., 2001, AJ, 121, 10
Dawson W. A., 2013, ApJ, 772, 131
De Lucia G., Springel V., White S. D. M., 2006, MNRAS, 366, 499
den Hartog R., Katgert P., 1996, MNRAS, 279, 349
Dressler A., Shectman S. A., 1988, AJ, 95, 985
Ebeling H., Voges W., Bohringer H., Edge A. C., Huchra J. P., Briel U. G., 1996, MNRAS, 281, 799
Fadda D., Girardi M., Giuricin G., Mardirossian F., Mezzetti M., 1996, ApJ, 473, 670
Fichett M. J., Webster R., 1987, ApJ, 317, 653
Fraley C., Raftery A. E., 2006, Technical Report, 504, Department of statiscs, University of Washington
Fujita Y., Koyama K., Tsuru T., Matsumoto H., 1996, PASJ, 48, 191
Fujita Y., Tawa N., Hayashida K., Takizawa M., Matsumoto H., Okabe N., Reiprich T. H., 2008, PASJ, 60, 343
Galli M., Cappi A., Focardi P., Gregorini L., Vettolani G., 1993, A&AS, 101, 259
Girardi M., Demarco R., Rosati P., Borgani S., 2005, A&A, 436, 29
Gregory S. A., Thompson L. A., 1984, ApJ, 286, 422
Hansen S. H., Egli D., Hollenstein L., Salzmann C., 2005, New Astron., 10, 379
Hansen S. H. et al., 2006, J. Cosmol. Astropart. Phys., 01, 014
Hartigan J. A., Hartigan P. M., 1985, Annu. Stat., 13, 70
Heisler J., Tremaine S., Bahcall J. N., 1985, ApJ, 298, 8
Hjorth J., Williams L. L. R., 2010, ApJ, 722, 851
Holzmann H., Vollmer S., 2008, Adv. Stat. Anal., 92, 57
Hou A., Parker L., Harris W. E., Wilman D. J., 2009, ApJ, 702, 1199
Huchra J. P., Geller M. J., 1982, ApJ, 257, 423
Hwang H. S., Lee M. G., 2007, ApJ, 662, 236
Ihaka R., Gentleman R., 1996, J. Comput. Graph. Stat., 5, 299
Jee M. J., White R. L., Benítez N., Ford H. C., Blakeslee J. P., Rosati P., Demarco R., Illingworth G. D., 2005a, ApJ, 618, 46
Jee M. J., White R. L., Ford H. C., Blakeslee J. P., Illingworth G. D., Coe D. A., Tran K.-V. H., 2005b, ApJ, 634, 813
Jee M. J. et al., 2007, ApJ, 661, 728
Jones D. H. et al., 2009, MNRAS, 399, 683
Katayama H., Hayashida K., Hashimotodani K., 2001, PASJ, 53, 1133
Kato Y., Nakazawa K., Gu L., Akahori T., Takizawa M., Fujita Y., Makishima K., 2015, PASJ, 67, 71
Krause M. O., Ribeiro A. L. B., Lopes P. A. A., 2013, A&A, 551, A143
Kravtsov A. V., Borgani S., 2012, ARA&A, 50, 353
Kurtz M. J., Mink D. J., 1998, PASP, 110, 934
Landolt A. U., 1992, AJ, 104, 340
Lazzati D., Chincarini G., 1998, A&A, 339, 52
Lee K. L., 1979, J. Amer. Statist. Assoc., 74, 708
Liao S., Cheng D., Chu M.-C., Tang J., 2015, ApJ, 809, 64
Li L.-X., 1998, Gen. Rel. Gravit., 30, 3
Lopes P. A. A., de Carvalho R. R., Kohl-Moreira J. L., Jones C., 2009, MNRAS, 399, 2201
Lynden-Bell D., 1967, MNRAS, 136, 101
Mahdavi A., Hoekstra H., Babul A., Balam D. D., Capak P. L., 2007, ApJ, 668, 806
Manolopoulou M., Plionis M., 2016, preprint (arXiv:1604.06256v2)
Markevitch M., Govoni F., Brunetti G., Gerius D., 2005, ApJ, 627, 733
Merrall T. E. C., Henriksen R. N, 2003, ApJ, 595, 43
Naab T., Johansson P. H., Ostriker J. P., 2007, ApJ, 658, 710
Nolthenius R., White S. D. M., 1987, MNRAS, 225, 5050
Nusser A., 2008, MNRAS, 384, 343
Oegerle W. R., Hill J. M., 1992, AJ, 104, 6
Ogorodnikov K. F., 1957, Sov. Astron., 1, 748
Owers M. S., Nulsen P. E. J., Couch W. J., Markevitch M., Poole G. B., 2009, ApJ, 692, 702
Owers M. S., Nulsen P. E. J., Couch W. J., 2011, ApJ, 741, 122
Pawl A., Evrard A. E., Dupke R. A., 2005, ApJ, 631, 773
Peebles P. J. E., 1993, Principles of Physical Cosmology. Princeton Univ. Press, Princeton, NJ
Pinkney J., Roettiger K., Burns J. O., Bird C. M., 1996, ApJS, 104, 1
Ramella M. et al., 2007, A&A, 470, 39
Ribeiro A. L. B., Lopes P. A. A., Trevisan M., 2011, MNRAS, 413, L81.
Ribeiro A. L. B., de Carvalho R. R., Trevisan M., Capelato H. V., La Barbera F., Lopes P. A. A., Schilling A. C., 2013, MNRAS, 434, 784
Ricker P. M., 1998, ApJ, 499, 670
Ricker P. M., Sarazin C. L., 2001, ApJ, 561, 621
Smith G. P. et al., 2010, MNRAS, 409, 169
Springel V., White S. D. M., Jenkins A., 2005, Nature, 435, 629
Takizawa M., 2000, ApJ, 532, 183
Teague P. F., Carter D., Gray P. M., 1990, ApJS, 72, 715
Tonry J., Davis M., 1979, AJ, 84, 1511
Ueda H., Itoh M., Suto Y., 1993, ApJ, 408, 3
van Dokkum P. G., 2001, PASP, 113, 1420
Voit G. M., 2005, Rev. Mod. Phys., 77, 207
Wainer H., Shacht S., 1978, Psichometrika, 43, 203
Werner N., Finoguenov A., Kaastra J. S., Simionescu A., Dietrich J. P., Vink J., Bööhringer H., 2008, A&A, 482, L29
West M. J., Bothun G. D., 1990 ApJ, 350, 36
West M. J., Oemler A., Dekel A., 1988, ApJ, 327, 1
Wing J. D., Blanton E. L., 2013, ApJ, 767, 102
Wojtak R., Lokas E. L., Mamon G. A., Gottlöber S., Klypin A., Hoffman Y., 2008, MNRAS, 388, 815
Yahil A., Vidal N. V., 1977, ApJ, 214, 347

APPENDIX A: TABLES A1 AND A2

Tables A1 and A2 present the properties obtained with the RVSAO and o XCSAO tasks, and the magnitudes, listed in column 3, obtained from SExtractor aperture magnitude with an aperture of 3.2 arcsec, for both cluster.

Table A1. Abell 3407.

RA (J2000) (1)	Dec. (J2000) (2)	m_R (3)	V (km s^{-1}) (4)	$R_{\rm quality}$ (5)	Emission lines (6)
7:03:28.36	−49:10:49.3	17.90	49 440 ± 70	4.90	–
7:03:37.58	−49:03:31.8	14.40	12 865 ± 28	14.01	–
7:03:39.11	−48:59:29.9	17.01	13 756 ± 28	14.06	–
7:03:42.36	−49:01:46.3	16.99	12 926 ± 33	10.60	–
7:03:44.49	−48:59:08.5	17.34	14 551 ± 38	7.45	H β, H α, N II
7:03:47.94	−48:58:25.8	18.21	12 597 ± 39	3.51	O II, H β, H α, N II
7:03:48.57	−49:08:24.6	17.05	12 804 ± 29	9.28	–
7:03:49.09	−49:18:49.0	18.27	12 215 ± 85	3.30	H β, O III, O III, H α, N II, S I
7:03:52.41	−49:09:55.1	18.75	49 787 ± 55	5.71	–
7:03:53.70	−49:06:54.3	17.23	12 615 ± 38	4.67	–
7:03:55.17	−49:03:41.6	18.39	13 620 ± 39	3.46	H β, H α, N II
7:03:58.00	−49:04:50.0	14.23	12 885 ± 42	17.74	–
7:03:59.45	−49:05:12.9	14.70	12 621 ± 26	7.32	O I, H α
7:04:03.92	−49:05:59.8	16.53	13 304 ± 22	18.20	–
7:04:04.34	−49:20:45.5	17.25	13 215 ± 37	5.49	O I
7:04:05.96	−48:54:31.4	18.27	56 185 ± 53	3.61	–
7:04:08.56	−49:03:32.3	18.22	49 744 ± 36	5.71	O III, O III
7:04:09.02	−49:10:35.3	17.17	11 623 ± 29	9.73	–
7:04:11.68	−49:13:17.4	17.78	49 463 ± 34	7.40	–
7:04:23.14	−49:14:01.2	18.61	49 454 ± 88	3.90	–
7:04:24.92	−49:20:47.1	16.83	− 1 ± 43	4.55	O II, O I
7:04:25.97	−48:45:43.3	16.38	13 858 ± 37	9.68	O II, O III
7:04:27.02	−49:06:49.1	16.77	12 857 ± 28	11.65	O II, O I
7:04:30.11	−49:10:54.1	17.36	11 613 ± 26	9.23	–
7:04:30.31	−48:47:03.2	15.78	13 138 ± 35	13.26	O I, S II
7:04:32.50	−49:03:12.6	18.51	12 589 ± 49	3.61	–
7:04:34.43	−48:59:35.6	17.70	76 ± 39	4.45	–
7:04:36.80	−49:04:31.9	17.15	11 951 ± 45	11.54	–
7:04:37.41	−49:01:29.8	18.43	11 966 ± 37	4.10	–
7:04:38.07	−48:58:57.1	16.55	12 820 ± 34	14.70	–
7:04:39.08	−48:49:48.6	18.17	13 481 ± 58	5.18	O I
7:04:42.24	−49:06:51.1	16.30	12 931 ± 24	19.67	–
7:04:43.40	−48:56:43.9	18.34	12 957 ± 93	3.60	–
7:04:43.93	−49:02:46.7	16.47	13 175 ± 29	12.93	–
7:04:46.94	−49:09:50.7	16.30	11 591 ± 33	14.55	–
7:04:47.05	−48:45:36.4	17.38	12 823 ± 56	5.37	O II
7:04:52.15	−49:05:51.3	17.10	12 105 ± 23	11.82	–
7:04:56.44	−49:06:18.8	17.61	10 733 ± 56	5.10	–
7:04:58.15	−49:02:31.6	17.38	32 285 ± 33	8.29	O III
7:04:58.58	−49:21:37.1	16.40	13 558 ± 33	12.92	O I
7:05:04.76	−49:00:18.5	17.43	11 867 ± 33	9.29	–
7:05:05.77	−48:51:08.1	17.24	12 439 ± 36	2.99	O II, H β, O III, O III, H α, N II
7:05:03.18	−49:06:01.5	18.24	11294 ± 36	5.54	–
7:05:09.45	−49:02:51.7	15.26	11289 ± 33	9.17	–
7:05:10.25	−49:00:17.6	17.68	12 229 ± 28	7.27	–
7:05:11.10	−48:53:35.2	17.46	21 859 ± 55	5.84	O II, H β, O III, O III
7:05:14.41	−49:17:15.6	17.78	32 419 ± 48	6.40	O III
7:05:13.18	−49:13:19.6	16.66	11 419 ± 26	11.16	–
7:05:16.07	−49:16:39.9	17.33	13 193 ± 42	5.60	O II, O III, O III, O I, H α
7:05:20.99	−49:07:34.6	17.98	11 360 ± 53	4.11	–
7:05:23.38	−49:00:12.5	17.69	12 602 ± 22	8.97	–
7:05:29.04	−49:07:40.8	16.08	12 113 ± 30	13.13	–
7:05:30.99	−48:58:19.0	18.56	21 833 ± 70	3.10	O II, H β, O III, O III
7:05:35.55	−49:04:14.0	17.51	11 718 ± 33	8.11	–
7:05:36.69	−49:19:57.9	17.23	13 538 ± 39	5.07	–
7:05:37.22	−49:17:17.2	17.86	41 646 ± 46	3.96	–
7:05:39.59	−48:45:15.6	16.70	12 693 ± 43	3.39	H β, O I, H α, N II
7:05:47.66	−48:57:40.2	14.63	12 567 ± 34	10.03	O II
7:05:49.42	−49:02:52.2	17.56	11 755 ± 42	7.08	–
7:05:55.46	−48:47:10.8	17.58	12 775 ± 116	3.30	O III
7:05:58.44	−49:15:00.5	17.10	11 959 ± 41	6.92	–

Table A1 *– continued*

RA (J2000) (1)	Dec. (J2000) (2)	m_R (3)	V (km s^{-1}) (4)	$R_{\rm quality}$ (5)	Emission lines (6)
7:06:01.47	−49:00:59.6	16.81	11 844 ± 41	6.71	–
7:06:11.81	−49:08:11.2	16.57	20 ± 41	5.86	–
7:06:14.75	−49:02:51.8	16.26	11 694 ± 28	11.61	O II, S I
7:06:19.08	−48:49:19.9	16.62	12 320 ± 54	5.53	O I
7:06:33.93	−49:04:25.4	17.45	12 858 ± 46	5.07	–
7:06:50.94	−49:04:09.3	17.26	11 897 ± 39	4.16	H α, N II, S I

Table A2. Abell 3408.

RA (J2000) (1)	Dec. (J2000) (2)	m_R (3)	V (km s^{-1}) (4)	$R_{\rm quality}$ (5)	Emission lines (6)
7:07:01.99	−49:19:49.9	16.48	13 207 ± 29	8.36	–
7:07:18.86	−49:25:58.3	18.89	37 652 ± 61	2.04	O II, O III, H β
7:07:20.40	−49:13:39.2	18.87	11 584 ± 115	2.60	–
7:07:24.17	−49:21:53.1	17.99	13 193 ± 65	2.00	O I, O II, O III, H α, H β, N II
7:07:25.88	−49:12:50.8	15.84	13 014 ± 44	6.32	–
7:07:26.27	−49:12:13.5	18.21	13 009 ± 35	5.31	–
7:07:33.05	−49:21:45.5	16.21	13 226 ± 29	8.33	O I,O II
7:07:34.36	−49:24:51.1	16.72	12 649 ± 33	5.74	–
7:07:36.08	−49:10:29.7	17.58	28 150 ± 32	6.42	–
7:07:38.37	−49:01:35.6	18.07	12 728 ± 62	2.65	O I, O II, O III, H α, H β, N II
7:07:39.38	−49:07:02.7	15.37	13 147 ± 24	9.84	–
7:07:39.50	−49:14:12.8	17.80	12 127 ± 28	6.82	–
7:07:45.19	−49:24:59.6	17.14	12 512 ± 36	6.21	–
7:07:52.22	−49:07:25.3	17.40	12 753 ± 30	8.33	–
7:07:59.17	−49:09:56.6	16.82	12 110 ± 26	11.50	–
7:07:59.46	−49:01:36.1	17.09	13 169 ± 44	4.40	–
7:07:59.59	−49:16:54.9	17.06	12 697 ± 37	9.00	–
7:08:06.10	−49:24:21.5	18.28	36 539 ± 61	3.01	–
7:08:06.84	−49:15:39.1	18.65	12 660 ± 83	2.60	O III, H α
7:08:08.82	−49:10:25.4	14.80	13 027 ± 29	6.00	–
7:08:10.60	−48:58:08.8	18.86	11 935 ± 75	1.80	O I, O II, H α, N II
7:08:11.06	−49:14:17.5	18.62	42 322 ± 48	3.90	–
7:08:11.44	−49:09:53.1	13.50	12 653 ± 24	12.98	–
7:08:14.25	−49:08:09.3	15.98	11 901 ± 40	13.85	–
7:08:16.75	−49:11:44.9	16.18	12 934 ± 25	9.47	–
7:08:21.71	−49:07:07.5	15.97	11 867 ± 26	9.25	O II
7:08:24.25	−49:11:49.1	17.37	13 524 ± 23	11.10	–
7:08:30.01	−49:20:07.6	16.72	13 281 ± 32	8.11	–
7:08:31.80	−49:06:46.3	16.54	10 772 ± 30	10.11	–
7:08:35.36	−49:12:59.6	16.70	11 458 ± 40	3.74	–
7:08:37.34	−49:08:19.7	18.23	12 793 ± 65	2.07	O I, O II, O III, H α, H β, N II
7:08:45.66	−49:03:02.9	17.33	12 168 ± 46	2.79	–
7:08:47.16	−49:13:05.6	17.57	13 610 ± 29	4.88	–
7:08:47.19	−49:17:29.5	17.77	21 830 ± 55	3.85	–
7:08:47.42	−49:00:14.4	18.86	46 739 ± 76	1.98	O II, O III, H β
7:08:55.32	−49:16:18.0	16.28	12 764 ± 32	7.32	–
7:08:56.03	−49:18:07.0	16.92	12 417 ± 32	5.68	–
7:10:18.03	−49:07:43.7	15.50	13 391 ± 42	3.29	–

This paper has been typeset from a TEX/LATEX file prepared by the author.